Accepted Manuscript

Design, synthesis and biological evaluation of novel 4-anilinoquinazoline derivatives as hypoxia-selective EGFR and VEGFR-2 dual inhibitors

Huiqiang Wei, Yuqing Duan, Wenfeng Gou, Jie Cui, Hongxin Ning, Deguan Li, Yong Qin, Qiang Liu, Yiliang Li

PII: S0223-5234(19)30676-2

DOI: https://doi.org/10.1016/j.ejmech.2019.07.055

Reference: EJMECH 11552

To appear in: *European Journal of Medicinal Chemistry*

Received Date: 6 May 2019

Revised Date: 10 July 2019

Accepted Date: 19 July 2019

Please cite this article as: H. Wei, Y. Duan, W. Gou, J. Cui, H. Ning, D. Li, Y. Qin, Q. Liu, Y. Li, Design, synthesis and biological evaluation of novel 4-anilinoquinazoline derivatives as hypoxia-selective EGFR and VEGFR-2 dual inhibitors, *European Journal of Medicinal Chemistry* (2019), doi: https://doi.org/10.1016/j.ejmech.2019.07.055.

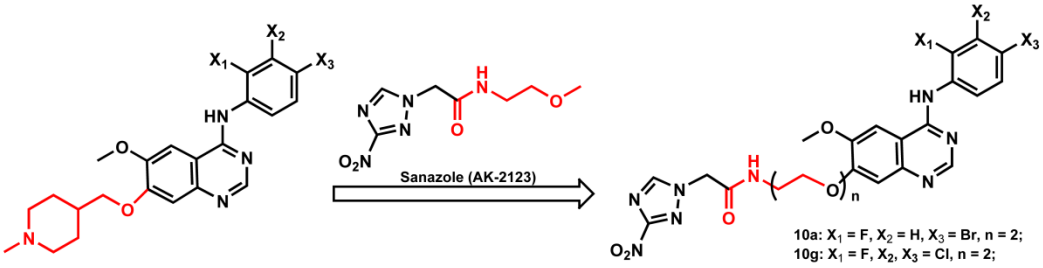

Vandetanib: X_1 = F, X_2 = H, X_3 =Br

	Kinase inhibition (IC_{50} nM)		Cell lines				A549 xenograft TGI (10 mg/kg, %)
			A549 (0.5 μM inhibition ratio, %)		H446 (0.5 μM inhibition ratio, %)		
	EGFR	VEGFR-2	normoxia	hypoxia	normoxia	hypoxia	
10a	5.90	36.78	6.75	75.86	18.95	84.37	63.9
10g	0.69	67.84	13.76	82.25	20.52	77.90	49.1

Novel TKIs with enhanced anti-tumor activity under hypoxia

Hypoxia is an inherent and significant difference between most solid tumors and healthy tissues. Herein, we designed a series of hypoxia-targeting TKIs to increase anti-tumor efficiency and reduce the adverse effects, by introducing 3-nitro-1,2,4-triazole moiety onto the EGFR/VEGFR-2 dual inhibitor vandetanib. Two lead compounds, 10a and 10g, demonstrated enhanced anti-tumor activities under hypoxia compared to vandetanib, which also shown enhanced inhibitory activities on tumor growth and reduced toxicities in tumor xenograft models compared to vandetanib and the vehicle control.

Design, synthesis and biological evaluation of novel 4-anilinoquinazoline derivatives as hypoxia-selective EGFR and VEGFR-2 dual inhibitors

Huiqiang Wei, [#,1] Yuqing Duan, [#,1] Wenfeng Gou,[1] Jie Cui,[2] Hongxin Ning,[1] Deguan Li,[1] Yong Qin,*[,3] Qiang Liu *[,1] and Yiliang Li *[,1]

[1] *Tianjin Key Laboratory of Radiation Medicine and Molecular Nuclear Medicine, Institute of Radiation Medicine, Peking Union Medical College & Chinese Academy of Medical Sciences, Tianjin 300192, China*

[2] *Tianjin University of Traditional Chinese Medicine, Tianjin 300193, China*

[3] *Department of Melanoma Medical Oncology, The University of Texas MD Anderson Cancer Center, Houston, TX, United States*

[#] These authors contributed equally to the article

*Corresponding authors: Yong Qin, Qiang Liu and Yiliang Li

Tel.: +86-22-8568-3040 (Y. Li)

E-mail: yongqin@mdanderson.org (Y. Qin); liuqiang@irm-cams.ac.cn (Q. Liu); liyiliang@irm-cams.ac.cn (Y. Li)

Abstract

Tyrosine kinase inhibitors (TKIs) have achieved substantial clinical effects for cancer treatment while causing a number of adverse effects. Since hypoxia is an intrinsic difference between solid tumor and healthy tissues, one strategy to overcome the adverse effects of TKIs is to enhance the specificity of anti-tumor activity by selectively targeting hypoxic region of tumors. Herein, we designed and synthesized a series of novel 4-anilinoquinazoline derivatives by introducing 3-nitro-1,2,4-triazole group to the side chain of vandetanib with modification of aniline moiety. Lead compounds, **10a** and **10g,** exhibited potent inhibitory activity against EGFR and VEGFR-2 kinase. Moreover, these two compounds were shown to enhance anti-proliferative activities on A549 and H446 cells under hypoxic conditions compared to vandetanib and dramatically down-regulate VEGF gene expression. *In vivo* studies confirmed that **10a** and **10g** not only inhibited tumor growth in A549 xenografts of BALB/c-nu mice but also significantly reduce toxicity associated with weight loss compared to vandetanib. These results suggest that EGFR/VEGFR-2 dual inhibitors, **10a** and **10g**, emerged as potential hypoxia-selective anti-tumor drugs with less toxicity for inhibiting *in vitro* and *in vivo* models of non-small cell lung cancer cells.

Keywords: Tyrosine kinase inhibitor ; 3-nitro-1,2,4-triazole ; Hypoxia; EGFR; VEGFR-2, Vandetanib

1. Introduction

A number of tyrosine kinase inhibitors (TKIs) have been developed as therapeutics for cancers and shown significant anti-tumor effects [1]. Among these tyrosine kinases, epidermal growth factor receptor (EGFR) and vascular endothelial growth factor receptor (VEGFR) are among those prominent targets. However, the clinical experience revealed that EGFR/VEGFR TKIs could induce unexpected serious toxic effects, such as cutaneous and oral adverse reactions, hypertension, arrhythmia, and diarrhea [2]. These toxicities of EGFR/VEGFR TKIs are mainly caused by the inhibition of EGFR/VEGFR signaling pathways in healthy tissues [3]. One feasible strategy to decrease or avoid adverse effects is to increase the specificity of TKIs against tumor cells. Hypoxia is a known inherent difference between solid tumors and healthy tissues, which represents a unique characteristic of a solid tumor that 10%-50% of tumor cells exist in a hypoxic microenvironment [4]. Hypoxia plays a crucial role in solid tumor survival and development. Previous studies have confirmed that hypoxia could promote the expression of various transcription factors, growth factors, and tyrosine kinase receptors, including hypoxia-inducible factor-1 (HIF-1), vascular endothelial growth factor (VEGF), platelet-derived growth factor-β (PDGF-β), and epidermal

growth factor receptor (EGFR). Most of these hypoxia-driven proteins can induce angiogenesis and accelerate the growth and migration of tumor cells through tyrosine kinase signaling pathways [5]. Moreover, hypoxia is one of the main reasons for radio- and chemotherapy resistance of solid tumors [6]. Thus, hypoxia is potentially exploitable in cancer treatment, and molecules in hypoxia-driven pathways, especially TKIs, represent attractive and feasible therapeutic "targets" to distinguish tumor from healthy tissues.

For example, VEGFR inhibitors inhibit tumor angiogenesis to enhance blood vessels atrophy and tumor hypoxia [7]. Thus, TKIs coupled with a hypoxia-targeted group, may improve the specificity of TKIs in tumor under hypoxia and overcome some adverse effects. Several studies have been conducted to discover potent hypoxia-targeted group for drug development. Cobalt compounds are one of these hypoxia-targeted candidates, which can be used to induce hypoxia in cell incubation due to the Co (III)/Co (II) redox potential [8]. In the absence of oxygen, Co (III) in drug-Co (III) complex would turn to Co (II) by a biochemical reduction. The reduced Co (II) showed significant ligand lability, and the drug was released after dissociation, which could be utilized as a hypoxia trigger in hypoxia-targeted prodrugs [9]. However, as a metallic element, the accumulation and metabolism of cobalt *in vivo* limited its application as the anti-cancer drug. The electron-affinity compounds, nitroimidazole derivatives, have been developed as hypoxia-activated and radiosensitizing agents in chemotherapy since the 1960s. 2-nitroimidazole group was used in several drug designs as the hypoxia-selective trigger, including the phosphoramidate mustard prodrug TH-302 (Evofosfamide, phase III) [10]. The 4-aminoquinazoline pharmacophore was widely used as an EGFR/VEGFR kinase inhibitor in the past few years [11]. In our previous research, a series of novel nitroimidazole-substituted 4-anilinoquinazoline derivatives were developed by coupling with EGFR/VEGFR-2 dual inhibitor vandetanib (Zactima®, **Figure 1**). The lead compound LYL-10 (**16f** in ref [12], **Figure 1**) from this study showed an increase of anti-tumor activity under hypoxia than normoxia [12]. However, the high electron-affinity of nitroimidazole derivatives also contributes to their potential cytotoxicity [13] and poor pharmacokinetic properties [14] of nitroimidazole, which limit its druggability. The toxicity of candidate compound LYL-10 was observed in previous *in vivo* study, and adverse reactions of vomit, diarrhea, asthenia, weight loss, and apparent abdominal breathing were documented in more than half of the test BALB/c-nu mice. Hence, nitroimidazole may not be an ideal candidate to construct hypoxia-selective drugs TKIs. Sanazole (AK-2123, **Figure 1**), a 3-nitro-1,2,4-triazole derivative, showed similar radio-sensitizing activities and much lower cytotoxicity than other 2-nitroimidazoles analogs, which had been tested as a radiosensitizer in Phase III clinical trials in radiotherapy for solid tumor [15]. It indicated that 3-nitro-1,2,4-triazole had the characteristic of an effective hypoxia-targeted group with good biosecurity and pharmacokinetic property.

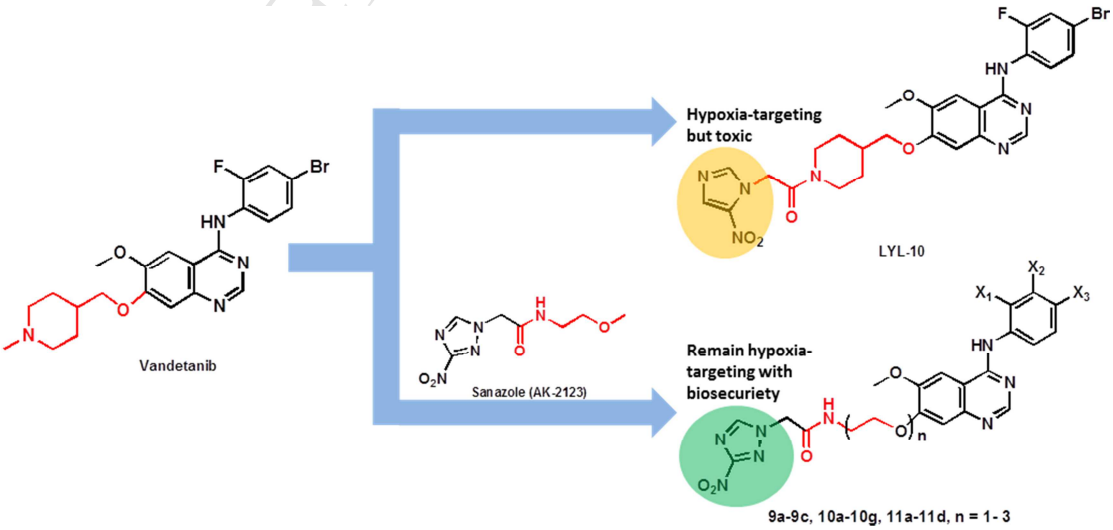

Figure 1. Structures of vandetanib, LYL-10, AK-2123 and target compounds

In this study, we developed a series of novel hypoxia-targeted EGFR/VEGFR-2 inhibitors with 3-nitro-1,2,4-triazole motif. To our knowledge, this is the first study to develop a hypoxia-selective TKI harboring EGFR/VEGFR-2 inhibitory activity of vandetanib, which may reduce the level of active compound in non-malignant tissue resulting in the decrease of the adverse effects while enhancing the inhibitory effect on tumor cells under hypoxia. Moreover, two lead compounds **10a** and **10g** were identified as potent candidates for cancer therapy based on our initial screening and validation by in vitro and in vivo models.

2. Results and Discussion

2.1 Design and synthesis of novel hypoxia-selective EGFR/VEGFR-2 inhibitor

Our previous research confirmed that introducing nitroimidazole groups onto the side chain of 4-anilinoquinazoline scaffold did not affect its EGFR/VEGFR-2 inhibitory activities[12]. In a similar strategy, 3-nitro-1,2,4-triazole moiety (AK-2123) was linked to the 4-anilinoquinazoline scaffold by long ether chains (**Figure 1**). This long ether side chain was also found in erlotinib and gefitinib [16]. The relationship between substitutions on the benzene ring and derivative activities has been discussed in our previous work [12], which provided a stragtegy to modify 4-anilinoquinazoline for develeoping novel EGFR/VEGFR-2 dual inhibitor. Hence, in this study, we selected representative substitutions to obtain several target compounds, which were further evaluated by various *in vitro* and *in vivo* cancer models.

Fourteen target compounds were designed and synthesized by seven steps as shown in **Scheme 1**, which were started from 7-benzyloxy-6-methoxy-3*H*-quinazolin-4-one (**1**) and 3-nitro-1,2,4-triazole (**5**). The intermediate 7-benzyloxy-4-chloro-6-methoxy-quinazoline (**2**) was obtained from **1** by refluxing in thionyl chloride and then reacted with anilines in isopropanol to give crude products of **3a-4g**, which were further treated by trifluoroacid to deprotect benzyl group at 80 °C, then adjusted pH to 10 by ammonium hydroxide [17]. These steps led to the production of white to yellow powders of intermediates **4a-4g** with moderate yields of 75%–88%. The intermediate methyl 2-(3-nitro-[1,2,4]triazol-1-yl)acetate (**6**) was prepared as yellow solid from **5** and methyl chloroacetate in the presence of a base (K_2CO_3) in refluxing acetonitrile with a good yield of 95.1%. The amide intermediate **7a-7c** were prepared from **6** and amino polyethylene glycols by aminolysis reaction in refluxing methanol with acceptable yields varying from 43.8%–86.7%. Sulfonylation of **7a-7c** was reacted in pyridine at 0 °C with a catalytic amount of 4-dimethylaminopyridine (DMAP). **8a-8c** were all faint yellow jellies with relatively lower yields of 20.8%–65.7%. Target compounds **9a-9c**, **10a-10g,** and **11a-11d** were obtained by intermediates **4a-4g** connecting with **8a-8c** in the presence of K_2CO_3 in DMF at 85 °C with moderate yields of 52.2%–68.9%. All of the target compounds were characterized by ^{1}H-NMR, ^{13}C-NMR, ^{19}F-NMR, and HRMS analysis.

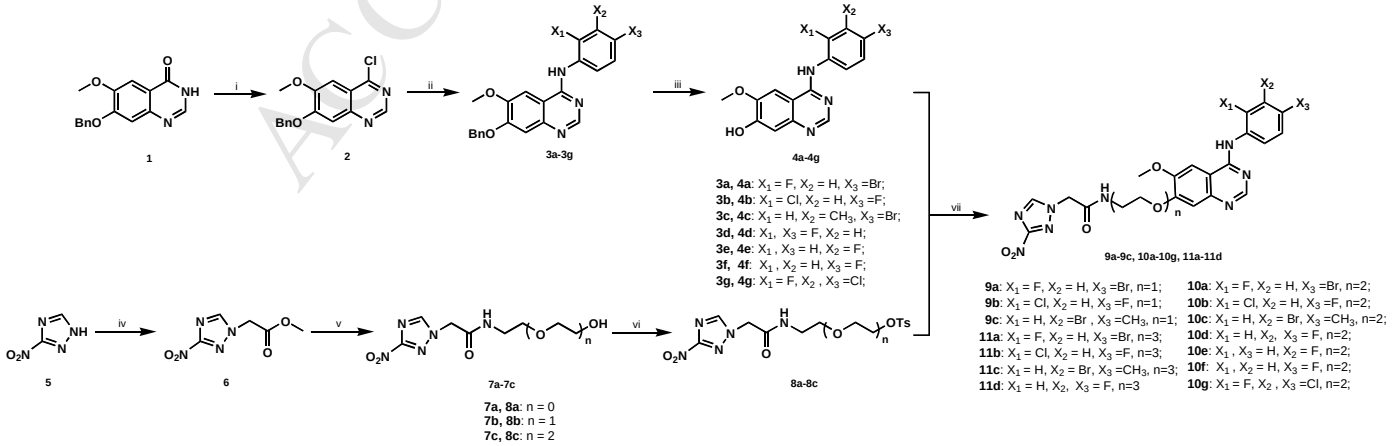

Scheme 1. Synthesis of target compounds. Reagents and conditions: (i) $SOCl_2$, DMF, reflux; (ii) Substituted anilines, *i*-PrOH, 60°C; (iii) TFA, 80°C, then ammonium hydroxide; (iv) Methyl chloroacetate, K_2CO_3,

acetonitrile, reflux; (v) amino polyethylene glycols, methanol, reflux; (vi) *p*-TsCl, DMAP, pyridine, 0°C to rt; (vii) K_2CO_3, DMF, 85°C

2.2 In vitro biological activities

The abilities of targeted compounds to inhibit EGFR and VEGFR-2 were evaluated by kinase inhibitory assay with LYL-10 and vandetanib as positive controls. As shown in **Table 1**, more than half of the tested compounds (LYL-10, **10a**, **10c**, **10d**, **10e**, **10g**, **11a**, **11b**, and **11c**) exhibited more potent EGFR inhibitory activities with the IC_{50} values ranging from 0.37 to 12.93 nM, which were superior to that of vandetanib (IC_{50} = 19.76 nM). Most of targeted compounds with a long link chain between 4-anilinoquinazoline and 3-nitro-1,2,4-triazole (n= 2 or 3; **10a**, **10c**, **10d**, **10e**, **10g**, **11a**, **11b**, and **11c**; IC_{50} from 0.37 to 12.93 nM) showed more potent inhibitory effects on EGFR than those compounds with a short side chain (n = 1; **9a**, **9b**, and **9c**; IC_{50} from 18.54 to 43.56 nM). It indicated that the length of the linker between trizole and quinazoline moiety could dramatically affect the EGFR inhibitory activity of targeted compounds. Most of the target compounds showed relatively enhanced inhibitory activities against VEGFR-2 kinase (IC_{50} from 36.78 to 4082.09 nM) than vandetanib. **10a** showed a similar inhibitory activity against VEGFR-2 kinase (IC_{50} = 36.78 nM) to vandetanib (IC_{50} = 33.26 nM). The IC_{50} values of **9a** and **10g** for VEGFR-2 were lower than 100 nM, but the rest of targeted compound showed a dramatically higher IC_{50} for VEGFR-2, which were about 5-122 folds of increases compared to vandetanib. Moreover, LYL-10 showed a slightly more potent inhibitory activity against VEGFR-2 with a 27.13 nM IC_{50} than vandetanib. It seemed that target compounds with bulky and heavy halogen atoms on aniline moiety exhibited better inhibitory activity to VEGFR-2 kinase, and the length of the link group also significantly impact the VEGFR-2 inhibitory activity. Several target compounds retained potent EGFR/VEGFR-2 inhibitory activities similar to vandetanib. Among these compounds, **10a** and **10g** demonstrated potent inhibitory activities against EGFR and VEGFR-2 with the IC_{50} values of 5.90/36.78 nM and 0.69/67.84 nM **(Figure 2). 10g** showed higher inhibitory activity against EGFR than VEGFR-2, since the IC_{50} value of **10g** against EGFR was 100-fold more potent than VEGFR-2. At the same time, **10g** still have potent inhibitory activity against VEGFR-2 with an IC_{50} lower than 70 nM, which was still in the same order of magnitude as vandetanib and LYL-10. Therefore, **10g** was still considered as an EGFR/VEGFR-2 dual inhibitor.

Table 1. *In vitro* EGFR and VEGFR-2 kinase inhibitory activity assay results of target compounds.

Compounds	Substituents				IC_{50} (nmol/L)	
	n	X_1	X_2	X_3	EGFR	VEGFR-2
9a	1	F	H	Br	43.56	86.84
9b	1	Cl	H	F	48.07	517.33
9c	1	H	Br	CH_3	18.54.	183.56
10a	2	F	H	Br	5.90	36.78
10b	2	Cl	H	F	20.83	4082.09
10c	2	H	Br	CH_3	0.37	407.47
10d	2	H	F	F	3.70	1104.22
10e	2	H	F	H	3.11	1196.59
10f	2	H	H	F	16.43	864.18
10g	2	F	Cl	Cl	0.69	67.84
11a	3	F	H	Br	4.95	216.77
11b	3	Cl	H	F	12.93	2865.05
11c	3	H	Br	CH_3	6.24	244.76

11d	3	H	F	F	19.97	1883.43
LYL-10	-	F	H	Br	3.23	27.13
vandetanib	-	F	H	Br	19.76	33.26

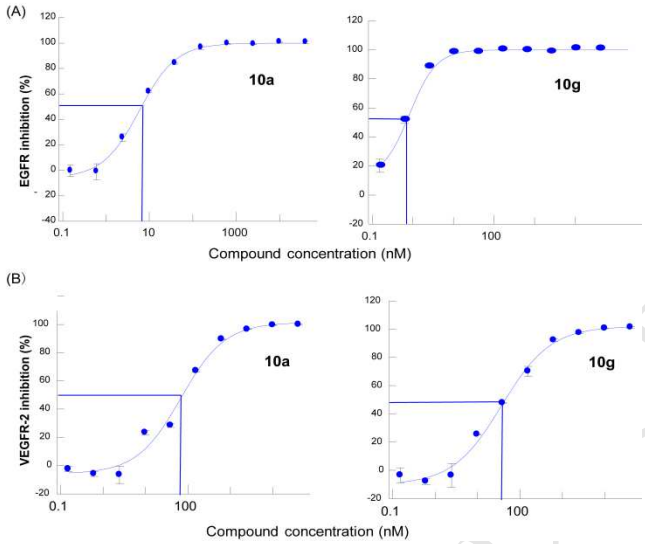

Figure 2. inhibition ratio curves of **10a** and **10g**: (A) EGFR; (B) VEGFR-2. Ten compound concentrations of 40000, 10000, 2500, 625, 156, 39, 10, 2, 1, and 0.2 nM were set in the assay.

The *in vitro* anti-proliferative effects of target compounds were evaluated against the A549 (adenocarcinomic human alveolar basal epithelial cells) and H446 (human small cell lung cancer cells) cell lines by using tetrazolium salt (WST-8) assay under normoxic or hypoxic conditions. The potential radio-sensitizing activities of targeted compounds were also evaluated under the hypoxic condition with the exposure dose of 8 Gy. Under normoxic conditions, 0.5 μM of target compounds, **9a**, **10a**, **10b**, **10c**, **10f**, **10g**, or **11a**, inhibited about 5~20% of cell growth for both cancer cell lines, which was less potent than vandetanib that inhibited 21.06% and 25.58% of cell growth in A549 and H446 cells (**Table 2** and **Figure 3 A-B**). Under hypoxic conditions, target compound, **10a**, exhibited stronger anti-proliferative activities (75.86% of inhibition in A549 cells and 84.37% of inhibition in H446 cells) in both cell lines than vandetanib (67.26% of inhibition in A549 cells and 77.67% of inhibition in H446 cells) (**Table 2** and **Figure 3 A-B**). Moreover, under hypoxic condition combining with irradiation, **10a** was the only compound that showed stronger inhibitory effects on the growth of both cancer cell lines than vandetanib (**Table 2** and **Figure 3 A-B**).

In order to estimate the hypoxic hypoxia-enhanced anti-tumor activities of tested compounds, the inhibitory activities caused by $CoCl_2$ and irradiation alone need to be taken out. Herein two kinds of hypoxic sensitive enhancement ratios, $HSER_{hyp}$ and $HSER_{hyp+IR}$, were used to quantitatively evaluate the enhanced inhibitory activities in normoxia/hypoxia and hypoxia/hypoxia+irradiation respectively (**Table 2** and **Figure 3 C-D**). All target compounds demonstrated evidently higher $HSER_{hyp}$ values (1.07~1.36) than vandetanib ($HSER_{hyp}$ = 1.05) on A549 and H446 cells, and target compounds, **10a** and **10g**, exhibited the best $HSER_{hyp}$ values of 1.32 and 1.36 on A549 cells; however, when combined with irradiation, tested compounds and vandetanib showed similar lower $HSER_{hyp+IR}$ values (0.80~0.96) on both A549 and H446 cells (**Table 2** and **Figure 3 C-D**). Target compounds containing 3-nitro-1,2,4-triazole moiety, **10a** and **10g**, demonstrated more potent hypoxia-targeted inhibitory activities than vandetanib on the growth of A549 and H446 cells under hypoxic conditions. Moreover, these two target compounds only showed additive effect with irradiation. No synergistic radio-sensitizing activities were observed in these assays.

Further quantitative polymerase chain reaction (Q-PCR) analysis showed that treatment of A549 cells with 5

μM of vandetanib, **10a**, or **10g** could down-regulate VEGF expression under normoxic or hypoxic conditions (**Table 3** and **Figure 4**). Both targeted compounds, **10a** and **10g**, demonstrated more potent inhibitory effects on VEGF expression in A549 cells compared to vandetanib.

Table 2. *In vitro* anti-proliferative activity assay results (inhibition ratios and *HSER*) in normoxia, hypoxia and hypoxia + irradiation

Compounds	Cell line	Inhibition ratios（%）			$HSER_{hyp}$ [c]	$HSER_{hyp+IR}$ [c]
		normoxia	Hypoxia [a]	hypoxia + IR [b]		
vandetanib	A549	21.06	67.26	81.44	1.05	0.94
	H446	25.58	77.67	82.02	1.04	0.88
9a	A549	14.87	72.99	80.31	1.19	0.90
	H446	16.76	76.34	79.03	1.07	0.85
10a	A549	6.75	75.86	86.41	1.32	0.96
	H446	18.95	84.37	88.66	1.17	0.93
10b	A549	10.33	69.01	77.88	1.17	0.89
	H446	13.87	80.31	83.35	1.14	0.89
10c	A549	5.48	65.39	69.18	1.15	0.80
	H446	18.65	77.71	80.10	1.08	0.86
10f	A549	8.43	72.53	76.94	1.25	0.86
	H446	11.08	78.70	80.58	1.13	0.86
10g	A549	13.76	82.25	80.70	1.36	0.87
	H446	20.52	77.90	85.04	1.07	0.91
11a	A549	16.04	74.36	80.36	1.20	0.90
	H446	20.38	78.81	84.92	1.08	0.91

[a] Control group in hypoxia was performed with 200 μM $CoCl_2$ solution and blank group with corresponding amount of DMSO; [b] Irradiation was conducted at 24 h late after administration under the absorbed dose of 8 Gy, and then cultured for another 24 h before CCK-8 test; [c] $Ir_{CoCl_2}/Ir_{CoCl_2+IR}$ values in A549 and H446 group were 59.94%/64.13% and 65.84%/68.77%.

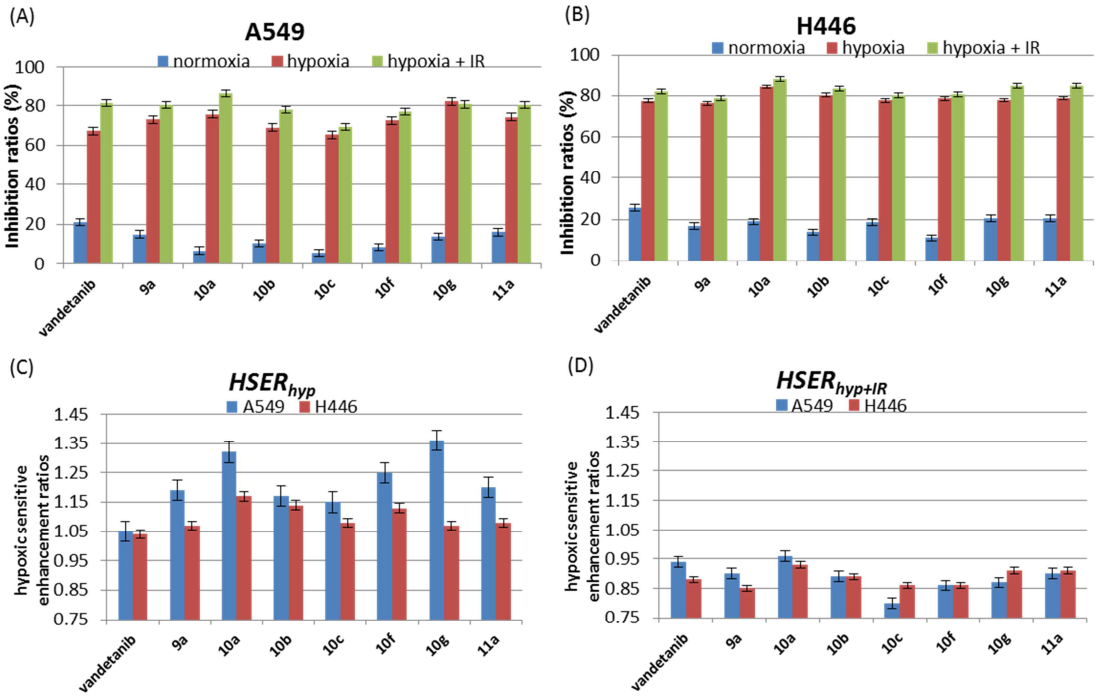

Figure 3. *In vitro* inhibition ratios in normoxia, hypoxia and hypoxia + irradiation on A549 (**A**) and H446 cells (**B**); *HSER* values of normoxia/hypoxia (**C**) and hypoxia/hypoxia+IR (**D**).

Table 3. VEGF gene expression level assay results of tested drugs in hypoxia/normoxia

Compounds	Control [b]	Vandetanib [c]	10a	10g
Normoxia	1.0000	0.6457	0.1571	0.1833
Hypoxia [a]	1.0000	0.2457	0.0011	0.0037

[a] hypoxia was performed with 200 μM $CoCl_2$ solution; [b] VEGF/EGF gene expression levels in control groups in hypoxia or normoxia was calculated as 1.0000, respectively and independently; [c] VEGF gene expression levels of vandetanib were from ref [12].

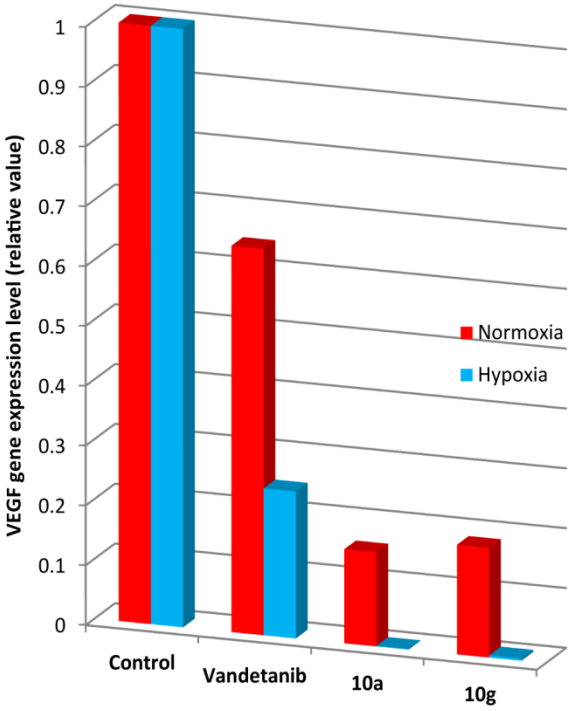

Figure 4. VEGF gene expression level assay results of tested compounds (5 μmol/L).

2.3. Molecular docking

In order to study the mechanism of target compound **10a** inhibiting the activity of relevant kinases, the molecular docking was conducted to analyze the different binding patterns of **10a** or vandetanib to EGFR or VEGFR-2 based on available crystal structures of these two receptor kinases (EGFR: PDB code 4I23 and VEGFR-2: PDB code 2RL5). As shown in **Figure 5A**, the structural modeling of the drug-protein complex showed that the binding pattern of **10a** to EGFR was similar to vandetanib, which the formation of important hydrogen bonds (H-bonds) between the backbone amino acid residue Met793 of EGFR and N1 atom of quinazoline moiety was observed in both drugs with similar H-bond distances (**10a**: 2.607 Å, vandetanib: 2.685 Å). Moreover, the aniline moieties of **10a** and vandetanib were observed to insert into EGFR`s hydrophobic pocket coplanarly, but the 3-nitro-1,2,4-triazole side chain of **10a** positioned in the solvent with no any additional H-bond with EGFR (**Figure 5A**). The structure model of **10a** and VEGFR-2 complex showed that the aniline moieties of **10a** and vandetanib occupied the narrow and deep hydrophobic pocket of VEGFR-2, and two critical H-bonds formed between the backbone amino acid residue Cys919 of VEGFR-2 and quinazoline N1 atom of drugs with the distances of 3.101 Å (**10a**) and 3.095 Å (vandetanib) (**Figure 5B**). Unlike the coplanar binding mode of **10a** or vandetanib to EGFR, the 3-nitro-1,2,4-triazole side chain of **10a** folded as a U shape, which contributed to a π-π stacking interaction with the Phe1047 residue of VEGFR-2 and further stabilized this folding structure. Moreover, three additional H-bonds were formed between **10a** and VEGFR-2 (**Figure 5B**). An extra H-bond formed between quinazoline N2 atom of **10a** and the side chain hydroxyl group of Thr916 residue of VEGFR-2 with a distance of 3.281 Å, and another two H-bonds were found between the side chain carbonyl oxygen atom of **10a** and the backbone residue Asn923 of VEGFR-2 with a distance of 2.895 Å and 3.319 Å at the gate of hydrophobic pocket (**Figure 5B**).

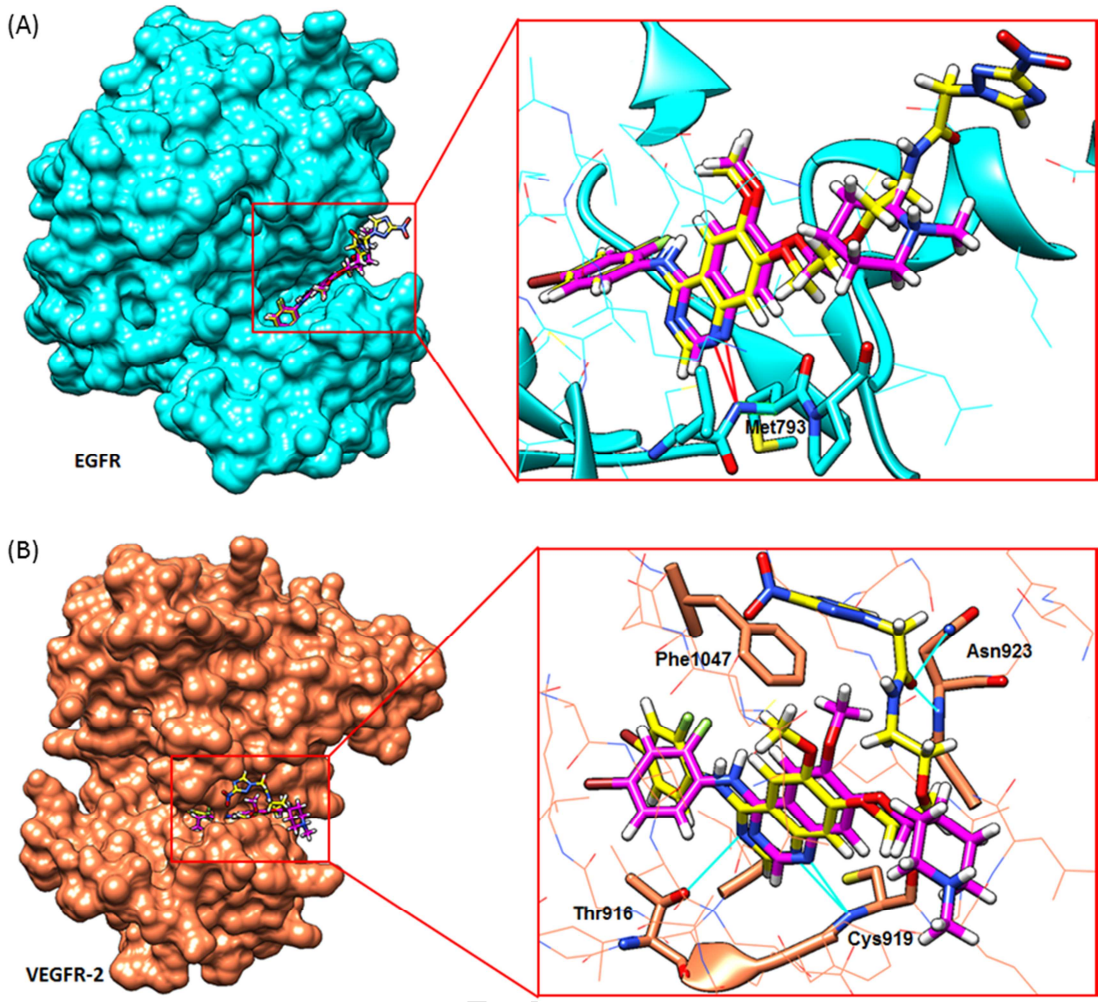

Figure 5. The docked poses of compound **10a** (C: yellow; N: blue; O: red) or vandetanib (C: magenta; N: blue; O: red) at the ATP binding cleft of EGFR kinase (cyan) (**A**), and VEGFR-2 kinase (coral) (**B**). H-bonds are shown in red lines (**A**) or sky-blue lines (**B**). The pictures were generated using Chimera. Some backbone amino acid residues were hidden.

A schematic diagram shown in **Figure 6** was given to illustrate how substituents and link group length influenced the binding between compounds and VEGFR-2 protein. As shown in **Figure 6**A, bulky and heavy halogen atoms (Br or Cl) on aniline moieties of compounds contributed more hydrophobicity and electronegativity than fluorine atoms or methyl groups, which caused a reinforced affinity for binding to VEGFR-2, especially when it fits into the narrow and deep hydrophobic pocket of VEGFR-2. Since the triazole side chain of compounds situated at the solvent portion, advisable bulky and heavy halogen atoms on aniline would balance the "barycenter" of target compounds and stabilized it in the complex. Target compounds with 4-bromo-2-fluoro- and 3,4-dichloro-2-fluoro- substituted aniline moieties showing higher VEGFR-2 kinase inhibitory activities were attributed to that the substitutions were bulky and heavy enough to balance the barycenter as well as afforded appropriate hydrophobicity and electronegativity to reinforce the binding complex **(Figure 6A)**. The length of the link group between 3-nitro-1,2,4-triazole and quinazoline also influenced the binding pattern. Triazole moiety in **10a** with appropriate length (n=2) contributed to the binding between **10a** and VEGFR-2, which formed a U shape structure like a fishhook to further stabilize drug-protein interaction by the formation of key H-bonds **(Figure 6A)**. This special U shape structure was believed to improve the affinity of targeted compound **10a** binding to VEGFR-2. The short linking group (n=1) of **9a** could prevent the formation of U shape structure resulting in the

triazole group of the drug blocking the gate of hydrophobic pocket and reducing the formation of H-bonds to stabilize the complex **(Figure 6B)**. With a longer link group (n⩾3), the triazole group of the drug would be impacted by solvent effect and shift the "barycenter" to the solvent region, which was detrimental to a stable drug-protein complex **(Figure 6C)**; Longer link groups also contributed to the excess flexibility that might cause unexpected pernicious influence, such as hERG potassium channel inhibition [18].

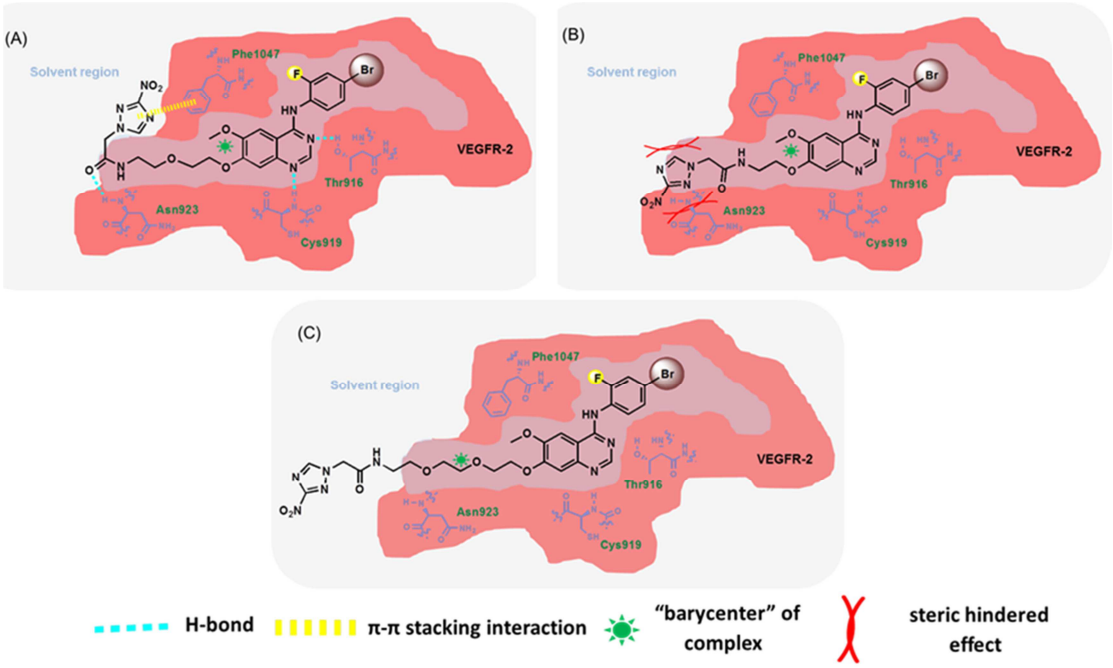

Figure 6. (**A**) Bulky and hydrophobic halogen atoms of aniline moiety reinforced the binding complex; the appropriate linking group length (n=2) contributed the "fishhook" binding pattern through a π-π stacking interaction and key H-binds formed with the residues Cys919, Asn923 and Thr916 of VEGFR-2. (**B**) The short linking group caused a sterically hindered effect at the opening of the hydrophobic pocket. (**C**) The long linking group shifted the "barycenter" to the solvent region, which resulted in an unstable drug-receptor complex.

Taking *in vitro* kinase inhibitory activities and docking study results into account, the preliminary structure-activity relationships (SAR) were obtained: the length of linking group impacts activities dramatically, and a proper length (n=2) was favorable to keep EGFR/VEGFR-2 inhibition; substituent on aniline was vital to VEGFR-2 selectivity, and advisable bulky and heavy halogen atoms substituted anilines were conducive to EGFR/VEGFR-2 inhibitory activities. More compound structure optimization would be undertaken according to the SAR guideline in the future.

2.4 In vivo anticancer activity

The targeted compounds, **10a** and **10g,** were selected to further investigate their anticancer activity in mouse modes based on their high antiproliferative activity derived from *in vitro* studies. The ability of **10a** and **10g** to suppress tumor growth in the A549 tumor cell xenograft models were further compared to vandetanib. The male BALB/c-nu mice were randomly divided into the vehicle control group, the experimental groups (treated with **10a** or **10g**), and the positive control group (treated with vandetanib). Respectively, each group consisted of 5 tumor-bearing mice. The mice were treated with **10a**, **10g**, and vandetanib with oral administration of 10 mg/kg drugs daily for 17 days, and tumor size and the body weight of the mouse were measured daily. In *in vivo* dose-dependent anti-proliferation experiments, each group consisted of 3 tumor-bearing mice. The mice were treated with **10a** and **10g** with oral drug administrations of 5 mg/kg, 15 mg/kg and 50 mg/kg daily for 18 days, and

tumor size were measured at day 4, 6, 8, 11, 13, 15 and 18.

As shown in **Figure 7A**, **10a** exhibited remarkable inhibition on A549 tumor growth with a tumor growth inhibitions (TGI) of 63.93% at day 17 compared to controls. The TGI value of **10a** at day 17 was similar to that of vandetanib (TGI: 62.06%, **Figure 7A**), indicating that the *in vivo* antitumor activity of **10a** was similar to vandetanib. After treatment of 7 days, the tumor volume slowly increased in the **10a**, **10g**, and vandetanib groups, and the **10g** group showed a faster tumor growth than **10a** and vandetanib, which indicated that these compounds could not completely control tumor growth in A549 xenografts. **10g** still showed a distinct inhibitory effect on tumor growth (TGI=49.05% at day 17) compared to the vehicle control group. Thus, **10a** and **10g** remained potent inhibitory activities against A549 tumor growth in mouse models. Moreover, the tumor growth inhibitions of **10a** and **10g** were dose-dependent in A549 xenografts (Figure 7B). The highest TGI of 80.5% was observed in the mice treated with 50 mg/kg of **10a** at day 18. The TGI value of **10g** at day 18 were found to be 28.10%, 63.90%, 76.33% for treatment of 5 mg/kg, 15 mg/kg, and 50 mg/kg respectively, while those values of **10a** were 31.22%, 68.31%, and 80.55%. Evidently, the TGI values of **10g** were much lower than those of **10a**, indicating that the *in vivo* antitumor activity of **10g** was less potent than that of **10a** (**Figure 7B**).

The in vivo toxicity of targeted compounds **10a** and **10g** was evaluated in BALB/c-nu mice, using vandetanib as control. The mice were monitored for body weight change and clinical signs of toxicity. The tested mice were well tolerated with oral administrations of **10a** and **10g**, and no significant weight loss was observed during the treatment up to 17 days compared to the vehicle control group (**Figure 7C**). However, the mice in vandetanib group showed a notable weight loss during the first 8 days of treatment compared to the vehicle control group, while their weights were back on to normal gradually after day 9 (**Figure 7C**). The maximum tolerated dose (MTD) assessed for **10a** was 100 mg/kg (five times a week for two weeks with two days off for a weekend) on male BALB/c-nu mice, and the treated animals exhibited no clinically observable sign of toxicity or weight loss. The results suggested that targeted compounds, **10a** and **10g,** developed in this study had potent antitumor activity with lower toxicity in A549 mouse model, which presented novel and promising EGFR/VEGFR-2 inhibitors as anticancer reagents.

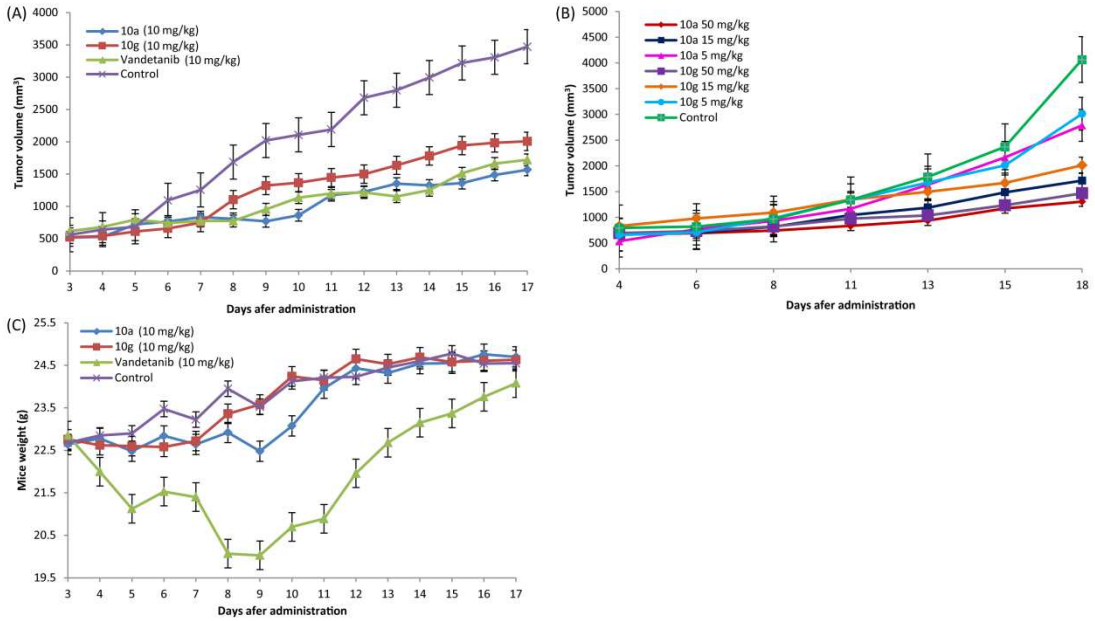

Figure 7. (**A**) Effect of compound **10a** and **10g** on tumor growth in A549 xenograft model; (**B**) Effect of administration dose on tumor growth in A549 xenograft model; (**C**) Mice weight changes during administration; A549 cells (1×10^7 cells) were implanted sc in the flank of BALB/c-nu mice. Seven days after implantation,

mice were orally administrated the tested doses daily, and the body weights of mice were measured daily.

3. Conclusions

In order to overcome the toxicity of LYL-10, which is a nitro-imidazole derivative of the EGFR/VEGFR-2 dual inhibitor vandetanib, we designed and synthesized a series of 3-nitro-1,2,4-triazole derivatives based on the structure of vandetanib as novel hypoxia-targeted antitumor compounds. The *in vitro* kinase inhibitory experiments showed that most of 3-nitro-1,2,4-triazole derivatives developed in this study retained potent EGFR inhibitory activities. Meanwhile, the lead compounds, **10a** and **10g,** exhibited potent VEGFR inhibitory activities that were similar to vandetanib. The molecular docking study confirmed that **10a** could bind with EGFR and VEGFR-2 with a great affinity. Further biological studies showed that most of the targeted compounds showed enhanced inhibitory activities in hypoxia towards A549 and H446 cells compared to vandetanib. Further gene expression assays confirmed that **10a** and **10g** could strongly inhibit the VEGF gene expression in A549 cells, which might contribute to the potent anti-proliferative activities of these two compounds in hypoxia. Based on *in vivo* anticancer test, **10a** and **10g** showed notable inhibitory effects and safety on tumor growth and good dose-dependence in dose-dependent anti-proliferation experiments in A549 xenograft models.

In conclusion, a series of novel 4-anilinoquinazoline TKIs were designed and synthesized. To our knowledge, this was the first study to introducing 3-nitro-1,2,4-triazole onto vandetanib to develop a potent EGFR/VEGFR-2 dual inhibitor with low toxicity targeted hypoxic solid tumors. The lead compounds, **10a** and **10g** were identified to be the most potent inhibitors by *in vitro* assays. **10a** and **10g** also showed prominent efficacy and drug safety in tumor xenograft models. Thus, **10a** and **10g** provide a foundation for further structure optimization and biological investigation to develop effective cancer therapeutic agent targeted hypoxic tumors.

4. Experimental Section

4.1 Chemical synthesis section

4.1.1 General

Reactions were monitored by thin-layer chromatography (TLC) using silica gel 60 UV254 pre-coated silica gel plates. Detection was using a UV lamp. Flash column chromatography was performed on 300–400 mesh silica gel. ^{1}H-NMR, ^{13}C-NMR, and ^{19}F-NMR were recorded on a BRUKER AVANCE III spectrometer (Bruker Ltd., Faellanden, Switzerland) at 600 MHz/151 MHz/564 MHz or an AV400 spectrometer at 400 MHz/100 MHz/376 MHz. Chemical shifts were reported in ppm using DMSO-d6 solution without TMS or $CFCl_3$ as internal standards. Mass spectra (ESI-MS) were performed on Agilent 1200 HPLC-6310 liquid chromatography mass spectrometer (Agilent Ltd., Palo Alto, CA, USA). High resolution mass spectrometry (HRMS) was performed on VG ZAB-HS gas chromatography mass spectrometer (VG Instruments Ltd., England). All reagents and solvents purchased from commercial sources without further purification.

4.1.2 Synthesis of methyl 2-(3-nitro-[1,2,4]triazol-1-yl)acetate (**6**)

11.41 g **5** (0.1 mol, 1 eq) and 15.29 g potassium carbonate (0.11 mol, 1.1 eq) was added to 100 mL acetonitrile and stirred at 50 °C for 0.5 h, the mixture turned to be bright yellow. 16.05 g methyl bromoacetate (0.105 mol, 1.05 eq) was added to the mixture and then reflux until no **5** appeared on TLC. The mixture was cooled to room temperature and filtrated. The filtrate was evaporated under reduced pressure, and the residue was dissolved in a mixture of ethyl acetate and water. The organic layer was separated and the aqueous layer was extracted twice. The organic extracts were combined, dried (anhydrous Na_2SO_4) and evaporated to dryness to afford 17.23 g **6** as brownish solid with the yield of 95.1%; ESI-MS m/z = 187.04 $[M + H]^+$; ^{1}H-NMR (400 MHz, DMSO-d_6): δ (ppm): 3.73 (s, 3H), 5.43 (s, 2H), 8.86 (s, 1H)

4.1.3 General synthetic procedure of *N*-polyethyleneglycol-2-(3-nitro-[1,2,4]triazol-1-yl)acetamide (**7a-7c**)

Dissolved 2.00 g **6** (10.74 mmol, 1 eq) and amino polyethylene glycol (2 eq) in methanol, heated to reflux and monitored the reaction by TLC. Evaporated solvent under reduced pressure after **6** consumed completely, the residue was purified by silica gel column chromatography to obtain **7a-c** (CH_2Cl_2:MeOH=30:1→15:1).

***N*-(2-hydroxy-ethyl)-2-(3-nitro-[1,2,4]triazol-1-yl)acetamide (7a).** Faint yellow solid powder with the yield of 81.2%; ESI-MS m/z = 215.16 $[M + H]^+$; ^{1}H-NMR (400 MHz, DMSO-d_6): δ (ppm): 3.17 (dd, J_1 = 5.6 Hz, J_2 = 11.6 Hz, 2H), 3.43 (dd, J_1 = 5.6 Hz, J_2 = 11.6 Hz, 2H), 4.73 (t, J = 5.6 Hz, 1H), 5.08 (s, 2H), 8.41 (t, J = 5.6 Hz, 1H), 8.82 (s, 1H)

***N*-[2-(2-hydroxy-ethoxy)ethyl]-2-(3-nitro-[1,2,4]triazol-1-yl)acetamide (7b).** Faint yellow oil with the yield 88.5%; ESI-MS m/z = 259.19 $[M + H]^+$; ^{1}H-NMR (400 MHz, DMSO-d_6): δ (ppm): 3.29 (m, 2H), 3.45 (m, 4H), 3.49 (m, 2H), 4.56 (t, J = 5.2 Hz, 1H), 5.10 (s, 2H), 8.44 (t, J = 5.2 Hz, 1H), 8.82 (s, 1H)

***N*-{2-[2-(2-hydroxy-ethoxy)-ethoxy]-ethyl}-2-(3-nitro-[1,2,4]triazol-1-yl)-acetamide (7c).** Faint yellow oil with the yield 68.5%; ESI-MS m/z = 303.21 $[M + H]^+$; ^{1}H-NMR (400 MHz, DMSO-d_6): δ (ppm): 3.28 (q, J = 5.6 Hz, 2H), 3.41-3.51 (m, 6H), 3.53 (m, 4H), 4.60 (t, J = 5.2 Hz, 1H), 5.11 (s, 2H), 8.49 (t, J = 5.2 Hz, 1H), 8.83 (s, 1H)

4.1.4 General synthetic procedure of (3-nitro-[1,2,4]triazol-1-yl)acetyl aminopolyethyleneglycol *p*-toluenesulfonate (**8a-8c**)

7a-c (1 eq) and DMAP (0.05 eq) were dissolved in 15 mL pyridine and stirred in ice bath for 0.5 h. TsCl (1.3 eq) was dissolved in 10 mL pyridine and then added dropwise to the reaction mixture in 1 h, then removed ice bath and stirred overnight. The mixture was extracted with ethyl acetate and 1 N HCl solution, organic layer was washed by 1 N HCl solution, water and brine, dried with anhydrous Na_2SO_4, then evaporated solvent. The residue was purified by silica gel column chromatography to obtain **8a-c** (hexane : ethyl acetate =3:1→1:2).

2-[2-(3-Nitro-[1,2,4]triazol-1-yl)-acetylamino]-ethyl *p*-toluenesulfonate (8a). Faint yellow jelly with the yield of 20.8%; ESI-MS m/z = 370.07 $[M + H]^+$; ^{1}H-NMR (400 MHz, DMSO-d_6): δ (ppm): 2.29 (s, 3H), 3.14 (q, J = 5.6 Hz, 2H), 4.63 (t, J = 5.6 Hz, 2H), 5.44 (s, 2H), 7.13 (d, J = 8.0 Hz, 2H), 7.50 (d, J = 8.0 Hz, 2H), 7.91 (t, J = 5.6 Hz, 1H), 8.89 (s, 1H)

2-{2-[2-(3-Nitro-[1,2,4]triazol-1-yl)acetylamino]ethoxy}ethyl *p*-toluenesulfonate (8b). Faint yellow jelly with the yield of 62.4%; ESI-MS m/z = 413.21 $[M + H]^+$; ^{1}H-NMR (400 MHz, DMSO-d_6): δ (ppm): 2.41 (s, 3H), 3.21 (dd, J_1 = 5.6 Hz, J_2 = 1.2 Hz, 2H), 3.38 (dd, J_1 = 5.6 Hz, J_2 = 11.2 Hz, 2H), 3.58 (t, J = 4.4 Hz, 2H), 4.12 (t, J = 4.4 Hz, 2H), 5.09 (s, 2H), 7.47 (d, J = 8.4 Hz, 2H), 7.78 (d, J = 8.0 Hz, 2H), 8.44 (t, J = 5.2 Hz, 1H), 8.82 (s, 1H)

2-(2-{2-[2-(3-nitro-[1,2,4]triazol-1-yl)-acetylamino]-ethoxy}-ethoxy)-ethyl *p*-toluenesulfonate (8c). Faint yellow jelly with the yield of 65.7%; ESI-MS m/z = 457.23 $[M + H]^+$; ^{1}H-NMR (400 MHz, DMSO-d_6): δ (ppm): 2.41 (s, 3H), 3.24-3.27 (m, 2H), 3.42 (t, J = 5.6 Hz, 2H), 3.45-3.50 (m, 2H), 3.58-3.60 (m, 2H), 3.64-3.75 (m, 2H), 4.12 (dd, J_1 = 3.6 Hz, J_2 = 5.2 Hz, 2H), 5.10 (s, 2H), 7.48 (d, J = 8.0 Hz, 2H), 7.78 (d, J = 8.0 Hz, 2H), 8.49 (t, J = 5.2 Hz, 1H), 8.83 (s, 1H)

4.1.5 General synthetic procedure of target compounds (**9a-9c**, **10a-10g** and **11a-11d**)

The quinazolinamines **4a-4g** (1 eq) was dissolved in 10 mL DMF, potassium carbonate (2 eq) was added and stirred at 50 °C for 0.5 h. Intermediate **8a-8c** (1 eq) was dissolved in DMF and then added dropwise to reaction mixture. The reaction was monitored by TLC. The mixture was cooled to room temperature after reactant consumed completely and then poured into water with stirring for 0.5 h. Filtrated and dissolved the precipitate with methanol, evaporated solvent under reduced pressure after dryness with anhydrous Na_2SO_4. The residue was recrystallized in methanol to obtain target compounds.

N-(2-{4-[(4-Bromo-2-fluorophenyl)amino]-6-methoxy-quinazolin-7-yl}oxy)ethyl-2-(3-nitro-[1,2,4]triazol-1-yl)acetamide (9a). Faint yellow solid powder with the yield of 47.2%; ESI-MS m/z = 561.07, 563.06 $[M+H]^+$;

GC-HRMS calcd for $C_{21}H_{18}BrFN_8O_5$, *m/z* = 561.0646, 563.0625 $[M+H]^+$, found: 561.0643, 563.0622; ^{1}H-NMR (600 MHz, DMSO-d_6): δ (ppm): 3.38 (dt, J_1 = 5.4 Hz, J_2 = 4.2 Hz, 2H), 3.96 (s, 3H), 4.32 (t, *J* = 4.2 Hz, 2H), 5.13 (s, 2H), 7.24 (s, 1H), 7.48 (d, 1H), 7.54 (t, 1H), 7.67 (d, 1H), 7.82 (s, 1H), 8.37 (s, 1H), 8.54 (t, *J* = 5.4 Hz, 1H), 9.55 (s, 1H); ^{13}C-NMR (151 MHz, DMSO-d_6): δ (ppm): 38.85, 52.52, 56.13, 68.95, 102.00, 107.74, 108.73, 117.48 (d, $^2J_{C\text{-}F}$ = 22.2 Hz), 119.21 (d, $^2J_{C\text{-}F}$ = 24.6 Hz), 126.39 (d, $^3J_{C\text{-}F}$ = 9.2 Hz), 127.44 (d, $^3J_{C\text{-}F}$ = 11.2 Hz), 129.46, 147.94 (d, $^1J_{C\text{-}F}$ = 210.1 Hz), 148.10, 152.93, 155.79, 156.88, 158.06, 161.91, 164.80; ^{19}F-NMR (376 MHz, DMSO-d_6) : δ (ppm): -115.42.

N-(2-{4-[(2-Chloro-4-fluorophenyl)amino]-6-methoxy-quinazolin-7-yl}oxy)ethyl-2-(3-nitro-[1,2,4]triazol-1-yl)acetamide (9b). Yellow solid powder with the yield of 67.1%; ESI-MS m/z = 517.12 $[M+H]^+$; GC-HRMS calcd for $C_{21}H_{18}ClFN_8O_5$, *m/z* = 517.1151 $[M+H]^+$, found: 517.1150; ^{1}H-NMR (400 MHz, DMSO-d_6): δ (ppm): 3.36 (t, *J* = 5.6 Hz, 2H), 3.96 (s, 3H), 4.34 (m, 2H), 5.15 (s, 2H), 7.25 (s, 1H), 7.31 (td, J_1 = 9.6 Hz, J_2 = 2.8 Hz, 1H), 7.58 (m, 2H), 7.84 (s, 1H), 8.34 (s, 1H), 8.57 (t, *J* = 5.2 Hz, 1H), 9.57 (s, 1H); ^{13}C-NMR (100 MHz, DMSO-d_6): δ (ppm): 39.34, 53.08, 56.59, 69.46, 108.54, 108.26, 109.01, 115.22 (d, $^2J_{C\text{-}F}$ = 21.2 Hz), 117.34 (d, $^2J_{C\text{-}F}$ = 24.6 Hz), 131.63 (d, $^3J_{C\text{-}F}$ = 9.1 Hz), 132.67 (d, $^3J_{C\text{-}F}$ = 11.2 Hz), 133.44, 147.20, 148.57, 149.31, 153.71 (d, $^1J_{C\text{-}F}$ = 212.1 Hz), 158.07, 159.13, 161.58, 162.46, 165.32; ^{19}F-NMR (376 MHz, DMSO-d_6) : δ (ppm): -114.11.

N-(2-{4-[(3-Bromo-4-methylphenyl)amino]-6-methoxy-quinazolin-7-yl}oxy)ethyl-2-(3-nitro-[1,2,4]triazol-1-y l)acetamide (9c). Faint green solid powder with the yield of 58.3%; ESI-MS m/z = 557.09, 559.09 $[M+H]^+$; GC-HRMS calcd for $C_{22}H_{21}BrN_8O_5$, *m/z* = 557.0897, 559.0876 $[M+H]^+$, found: 557.0899, 559.0879; ^{1}H-NMR (600 MHz, DMSO-d_6): δ (ppm): 2.33 (s, 3H), 3.35 (t, *J* = 5.6 Hz, 2H), 3.96 (s, 3H), 4.35 (m, 2H), 5.15 (s, 2H), 7.21 (s, 1H), 7.32 (d, 1H), 7.78 (m, 2H), 8.13 (s, 1H), 8.48 (s, 1H), 8.54 (t, *J* = 4.2 Hz, 1H), 8.83 (s, 1H), 9.45 (s, 1H); ^{13}C-NMR (151 MHz, DMSO-d_6): δ (ppm): 21.69, 38.98, 52.59, 56.24, 68.96, 101.95, 108.89, 121.11, 123.40, 124.83, 130.56, 131.49, 138.80, 146.89, 148.92, 152.68, 153.44, 156.03, 161.98, 164.80.

N-{2-[2-({4-[(4-Bromo-2-fluorophenyl)amino]-6-methoxyquinazolin-7-yl}oxy)ethoxy]ethyl}-2-(3-nitro-[1,2,4] triazol-1-yl)acetamide (10a). Faint yellow solid powder with the yield of 56.1%; ESI-MS m/z = 605.10, 607.09 $[M+H]^+$; GC-HRMS calcd for $C_{23}H_{23}BrFN_8O_6$, *m/z* = 605.0908, 607.0887 $[M+H]^+$, found: 605.0906, 607.0885; ^{1}H-NMR (600 MHz, DMSO-d_6): δ (ppm): 3.35 (t, *J* = 5.4 Hz, 2H), 3.58 (t, *J* = 5.4 Hz, 2H), 3.86 (t, *J* = 4.2Hz, 2H), 3.96 (s, 3H), 4.30 (t, *J* = 4.2 Hz, 2H), 5.13 (s, 2H), 7.24 (s, 1H), 7.48 (d, 1H), 7.54 (t, 1H), 7.67 (d, 1H), 7.82 (s, 1H), 8.37 (s, 1H), 8.55 (t, *J* = 5.4 Hz, 1H), 9.55 (s, 1H); ^{13}C-NMR (151 MHz, DMSO-d_6): δ (ppm): 38.96, 52.55, 56.11, 68.01, 68.46, 68.95, 102.00, 107.74, 108.72, 117.49 (d, $^2J_{C\text{-}F}$ = 22.2 Hz), 119.20 (d, $^2J_{C\text{-}F}$ = 24.6 Hz), 126.40 (d, $^3J_{C\text{-}F}$ = 9.2 Hz), 127.46 (d, $^3J_{C\text{-}F}$ = 11.2 Hz), 129.51, 147.90 (d, $^1J_{C\text{-}F}$ = 210.1 Hz), 148.08, 152.91, 155.79, 156.86, 157.46, 161.93, 164.75; ^{19}F-NMR (376 MHz, DMSO-d_6) : δ (ppm): -115.45.

N-{2-[2-({4-[(2-Chloro-4-fluorophenyl)amino]-6-methoxyquinazolin-7-yl}oxy)ethoxy]ethyl}-2-(3-nitro-[1,2,4] triazol-1-yl)acetamide (10b). Yellow solid powder with the yield of 64.1%; ESI-MS m/z = 561.13 $[M+H]^+$; GC-HRMS calcd for $C_{23}H_{22}ClFN_8O_6$ *m/z* = 561.1413 $[M+H]^+$, found: 561.1411; ^{1}H-NMR (400 MHz, DMSO-d_6): δ (ppm): 3.35 (t, *J* = 5.6 Hz, 2H), 3.59 (t, *J* = 5.6 Hz, 2H), 3.86 (m, 2H), 3.96 (s, 3H), 4.30 (m, 2H), 5.15 (s, 2H), 7.23 (s, 1H), 7.31 (td, J_1 = 9.6 Hz, J_2 = 2.8 Hz, 1H), 7.59 (m, 2H), 7.86 (s, 1H), 8.33 (s, 1H), 8.59 (t, *J* = 5.2 Hz, 1H), 9.57 (s, 1H); ^{13}C-NMR (100 MHz, DMSO-d_6): δ (ppm): 39.47, 53.06, 56.57, 68.49, 68.98, 69.47, 108.54, 108.25, 109.03, 115.18 (d, $^2J_{C\text{-}F}$ = 22.2 Hz), 117.31 (d, $^2J_{C\text{-}F}$ = 25.7 Hz), 131.69 (d, $^3J_{C\text{-}F}$ = 9.2 Hz), 132.69 (d, $^3J_{C\text{-}F}$ = 11.2 Hz), 133.43, 147.24, 148.60, 149.34, 153.73 (d, $^1J_{C\text{-}F}$ = 212.1 Hz), 158.11, 159.14, 161.59, 162.44, 165.28; ^{19}F-NMR (376 MHz, DMSO-d_6) : δ (ppm): -114.06.

N-{2-[2-({4-[(3-Bromo-4-methylphenyl)amino]-6-methoxyquinazolin-7-yl}oxy)ethoxy]ethyl}-2-(3-nitro-[1,2,4]triazol-1-yl)acetamide (10c). Green solid powder with the yield of 68.9%; ESI-MS m/z = 601.11 $[M+H]^+$; GC-HRMS calcd for $C_{24}H_{25}BrN_8O_6$ *m/z* = 601.1159, 603.1138 $[M+H]^+$, found: 601.1160, 603.1140; ^{1}H-NMR (600 MHz, DMSO-d_6): δ (ppm): 2.32 (s, 3H), 3.33 (t, *J* = 5.6 Hz, 2H), 3.57 (t, *J* = 5.6 Hz, 2H), 3.84 (t, *J* = 4.0 Hz,

2H), 3.96 (s, 3H), 4.30 (t, *J* = 4.0 Hz, 2H), 5.13 (s, 2H), 7.20 (s, 1H), 7.32 (d, 1H), 7.79 (m, 2H), 8.12 (s, 1H), 8.48 (s, 1H), 8.52 (t, *J* = 4.2 Hz, 1H), 8.83 (s, 1H), 9.43 (s, 1H); ^{13}C-NMR (151 MHz, DMSO-d_6): δ (ppm): 21.67, 38.99, 52.58, 56.21, 68.00, 68.48, 68.97, 101.91, 108.92, 121.09, 123.38, 124.84, 130.55, 131.47, 138.77, 146.87, 148.93, 152.68, 153.40, 156.02, 161.95, 164.76

N-{2-[2-({4-[(3,4-Difluorophenyl)amino]-6-methoxyquinazolin-7-yl}oxy)ethoxy]ethyl}-2-(3-nitro-[1,2,4]triazol-1-yl)acetamide (10d). Yellow solid powder with the yield of 58.9%; ESI-MS m/z = 545.17 $[M+H]^+$; GC-HRMS calcd for $C_{23}H_{22}F_2N_8O_6$ *m/z* = 545.1709 $[M+H]^+$, found: 561.1711; ^{1}H-NMR (400 MHz, DMSO-d_6): δ (ppm): 3.36 (t, *J* = 5.6 Hz, 2H), 3.59 (t, *J* = 5.6 Hz, 2H), 3.86 (m, 2H), 3.98 (s, 3H), 4.29 (m, 2H), 5.15 (s, 2H), 7.22 (s, 1H), 7.44 (dd, J_1 = 19.2 Hz, J_2 = 8.0 Hz, 1H), 7.60 (m, 1H), 7.84 (s, 1H), 8.08 (ddd, J_1 = 13.2 Hz, J_2 = 7.6 Hz, J_3 = 2.0 Hz, 1H), 8.50 (s, 1H), 8.58 (t, *J* = 5.6 Hz, 1H), 9.60 (s, 1H); ^{13}C-NMR (101 MHz, DMSO-d_6): δ (ppm): 39.46, 53.06, 56.72, 68.48, 68.95, 69.45, 102.40, 108.36, 109.34, 111.46 (d, $^2J_{C\text{-}F}$ = 21.2 Hz), 117.36 (d, $^2J_{C\text{-}F}$ = 17.7 Hz), 118.57, 137.13 (d, $^3J_{C\text{-}F}$ = 9.2 Hz), 145.73 (dd, $^1J_{C\text{-}F}$ = 241.4 Hz, $^2J_{C\text{-}F}$ = 12.7 Hz), 147.40, 148.60, 149.21 (dd, $^1J_{C\text{-}F}$ = 243.4 Hz, $^2J_{C\text{-}F}$ = 12.7 Hz), 149.43, 153.05, 153.94, 156.44, 162.43, 165.27; ^{19}F-NMR (376 MHz, DMSO-d_6) : δ (ppm): -137.77 (d, $^3J_{F\text{-}F}$ = 23.2 Hz), -145.10 (d, $^3J_{F\text{-}F}$ = 23.2 Hz).

N-{2-[2-({4-[(3-Florophenyl)amino]-6-methoxyquinazolin-7-yl}oxy)ethoxy]ethyl}-2-(3-nitro-[1,2,4]triazol-1-yl)acetamide (10e). Faint yellow solid powder with the yield of 57.1%; ESI-MS m/z = 527.18 $[M+H]^+$; GC-HRMS calcd for $C_{23}H_{23}FN_8O_6$ *m/z* = 527.1803 $[M+H]^+$, found: 527.1803; ^{1}H-NMR (400 MHz, DMSO-d_6): δ (ppm): 3.35 (dd, J_1 = 10.8 Hz, J_1 = 5.2 Hz, 2H), 3.59 (t, J = 5.6 Hz, 2H), 3.86 (m, 2H), 3.99 (s, 3H), 4.29 (m, 2H), 5.15 (s, 2H), 6.93 (td, J_1 = 8.4 Hz, J_2 = 2.0 Hz, 1H), 7.23 (s, 1H), 7.42 (dd, J_1 =15.2 Hz, J_2 = 8.0 Hz, 1H), 7.64 (d, 1H), 7.90 (m, 2H), 8.56 (s, 1H), 8.59 (t, J=5.2 Hz, 1H), 8.86 (s, 1H), 9.77 (brs, 1H); ^{13}C-NMR (101 MHz, DMSO-d_6): δ (ppm): 39.45, 53.05, 56.81, 68.55, 68.92, 69.44, 102.64, 107.68, 109.17, 109.39 (d, $^3J_{C\text{-}F}$ = 7.8 Hz). 110.18 (d, $^2J_{C\text{-}F}$ = 21.0 Hz), 118.18, 130.33 (d, $^3J_{C\text{-}F}$ = 9.5 Hz), 141.68 (d, $^2J_{C\text{-}F}$ = 11.2 Hz), 146.42, 148.60, 149.56, 152.72, 155.40 (d, $^1J_{C\text{-}F}$ = 254.4 Hz), 161.28, 162.43, 163.67, 165.27; ^{19}F-NMR (376 MHz, DMSO-d_6): δ (ppm): -112.68.

N-{2-[2-({4-[(4-Florophenyl)amino]-6-methoxyquinazolin-7-yl}oxy)ethoxy]ethyl}-2-(3-nitro-[1,2,4]triazol-1-yl)acetamide (10f). Faint yellow solid powder with the yield of 52.2%; ESI-MS m/z = 527.18 $[M+H]^+$; GC-HRMS calcd for $C_{23}H_{23}FN_8O_6$ *m/z* = 527.1803 $[M+H]^+$, found: 527.1805; ^{1}H-NMR (400 MHz, DMSO-d_6): δ (ppm): 3.35 (dd, J_1 = 10.8 Hz, J_2 = 5.2 Hz, 2H), 3.57 (t, *J* = 5.6 Hz, 2H), 3.85 (t, *J* = 4.0 Hz, 2H), 3.97 (s, 3H), 4.29 (m, 2H), 5.13 (s, 2H), 7.23 (m, 3H), 7.78 (dd, J_1 = 8.8 Hz, J_2 = 5.2 Hz, 2H), 7.83 (s, 1H), 8.43 (s, 1H), 8.56 (t, *J* = 5.2 Hz, 1H), 8.84 (s, 1H), 9.51 (s, 1H); ^{13}C-NMR (100 MHz, DMSO-d_6): δ (ppm): 39.45, 53.05, 56.84, 68.55, 68.92, 69.43, 102.66, 107.68, 109.17, 116.87 (d, $^3J_{C\text{-}F}$ = 6.6 Hz), 119.19 (d, $^2J_{C\text{-}F}$ = 18.4 Hz), 141.65, 146.42, 148.61, 149.46, 152.72 (d, $^1J_{C\text{-}F}$ = 252.4 Hz), 161.29, 162.45, 163.57, 166.07; ^{19}F-NMR (376 MHz, DMSO-d_6) : δ (ppm): -119.28.

N-{2-[2-({4-[(3,4-Dichloro-2-fluorophenyl)amino]-6-methoxyquinazolin-7-yl}oxy)ethoxy]ethyl}-2-(3-nitro-[1,2,4]triazol-1-yl)acetamide (10g). White solid powder with the yield of 52.2%; ESI-MS m/z=595.10 $[M+H]^+$; GC-HRMS calcd for $C_{23}H_{22}Cl_2FN_8O_6$, *m/z* = 595.1023 $[M+H]^+$, found: 595.1021; ^{1}H-NMR (400 MHz, DMSO-d_6): δ (ppm): 3.33 (t, *J* = 5.6 Hz, 2H), 3.57 (t, *J* = 5.6 Hz, 2H), 3.85 (m, 2H), 3.95 (s, 3H), 4.29 (m, 2H), 5.12 (s, 2H), 7.23 (s, 1H), 7.58 (m, 2H), 7.79 (s, 1H), 8.39 (s, 1H), 8.52 (t, *J* = 5.4 Hz, 1H), 8.83 (s, 1H), 9.69 (br.s., 1H); ^{13}C-NMR (400 MHz, DMSO-d_6): δ (ppm): 38.96, 52.56, 56.08, 68.06, 68.44, 68.95, 101.97, 107.71, 108.73, 119.58 (d, $^2J_{C\text{-}F}$ = 19.2 Hz), 125.26 (d, $^3J_{C\text{-}F}$ = 2.0 Hz), 126.74, 127.30 (d, $^2J_{C\text{-}F}$ = 13.1 Hz), 128.56, 146.88, 148.07, 149.05, 152.76, 153.04 (d, $^1J_{C\text{-}F}$ = 251.5 Hz), 153.65, 156.64, 161.93, 164.73; ^{19}F-NMR (376 MHz, DMSO-d_6) : δ (ppm): -113.48.

N-(2-{2-[2-({4-[(4-Bromo-2-fluorophenyl)amino]-6-methoxy-quinazolin-7-yl}oxy)ethoxy]ethoxy}ethyl)-2-(3-nitro-[1,2,4]triazol-1-yl)acetamide (11a). Faint yellow solid powder with the yield of 51.2%; ESI-MS m/z = 649.12, 651.12 $[M+H]^+$; GC-HRMS calcd for $C_{25}H_{26}BrFN_8O_7$, *m/z* = 649.1170, 651.1150 $[M+H]^+$, found: 649.1168, 651.1149; ^{1}H-NMR (400 MHz, DMSO-d_6): δ (ppm): 3.32 (t, *J* = 5.4 Hz, 2H), 3.58 (m , 4H), 3.86 (m,

4H), 3.96 (s, 3H), 4.35 (t, *J* = 4.2 Hz, 2H), 5.11 (s, 2H), 7.25 (s, 1H), 7.45 (d, 1H), 7.54 (t, 1H), 7.65 (d, 1H), 7.80 (s, 1H), 8.35 (s, 1H), 8.56 (t, *J* = 5.4 Hz, 1H), 9.54 (s, 1H); ^{13}C-NMR (100 MHz, DMSO-d_6): δ (ppm): 39.03, 52.57, 56.08, 68.10, 68.67, 68.86, 69.64, 69.91, 101.99, 107.78, 108.71, 117.56 (d, $^3J_{C\text{-}F}$ = 9.0 Hz), 119.33 (d, $^2J_{C\text{-}F}$ = 23.8 Hz), 126.40 (d, $^2J_{C\text{-}F}$ = 12.2 Hz), 127.52, 129.57, 147.92 (d, $^1J_{C\text{-}F}$ = 207.3 Hz), 148.13, 152.94, 153.57, 155.42, 156.89, 157.92, 161.90, 164.73; ^{19}F-NMR (376 MHz, DMSO-d_6) : δ (ppm): -115.55 (t, $^3J_{H\text{-}F}$ = 7.5 Hz).

N-(2-{2-[2-({4-[(2-Chloro-4-fluorophenyl)amino]-6-methoxy-quinazolin-7-yl}oxy)ethoxy]ethoxy}ethyl)-2-(3-nitro-[1,2,4]triazol-1-yl)acetamide (11b). Yellow solid powder with the yield of 54.9%; ESI-MS m/z = 605.17 $[M+H]^+$; GC-HRMS calcd for $C_{25}H_{26}ClFN_8O_7$ *m/z* = 605.1675 $[M+H]^+$, found: 605.1671; ^{1}H-NMR (400 MHz, DMSO-d_6): δ (ppm): 3.35 (t, *J* = 5.6 Hz, 2H), 3.56 (m, 4H), 3.87 (m, 4H), 3.96 (s, 3H), 4.29 (t, *J* = 4.2 Hz, 2H), 5.14 (s, 2H), 7.23 (s, 1H), 7.30 (td, J_1 = 9.6 Hz, J_2 = 2.8 Hz, 1H), 7.59 (m, 2H), 7.88 (s, 1H), 8.34 (s, 1H), 8.57 (t, *J* = 5.2 Hz, 1H), 9.58 (s, 1H); ^{13}C-NMR (100 MHz, DMSO-d_6): δ (ppm): 39.47, 53.06, 56.57, 68.49, 68.52, 68.98, 69.11, 69.46, 108.60, 108.23, 109.11, 115.16 (d, $^2J_{C\text{-}F}$ = 22.2 Hz), 117.29 (d, $^2J_{C\text{-}F}$ = 25.7 Hz), 131.68 (d, $^3J_{C\text{-}F}$ = 9.2 Hz), 132.60 (d, $^3J_{C\text{-}F}$ = 11.2 Hz), 133.38, 147.25, 148.57, 149.36, 153.72 (d, $^1J_{C\text{-}F}$ = 212.1 Hz), 158.10, 159.13, 161.57, 162.45, 165.32; ^{19}F-NMR (376 MHz, DMSO-d_6) : δ (ppm): -114.10.

N-(2-{2-[2-({4-[(3-Bromo-4-methylphenyl)amino]-6-methoxy-quinazolin-7-yl}oxy)ethoxy]ethoxy}ethyl)-2-(3-nitro-[1,2,4]triazol-1-yl)acetamide (11c). Faint green solid powder with the yield of 66.6%; ESI-MS m/z = 645.14, 647.13 $[M+H]^+$; GC-HRMS calcd for $C_{26}H_{29}BrN_8O_7$ *m/z* = 645.1421, 647.1400 $[M+H]^+$, found: 645.1423, 647.1401; ^{1}H-NMR (600 MHz, DMSO-d_6): δ (ppm): 2.30 (s, 3H), 3.35 (t, *J* = 5.4 Hz, 2H), 3.54 (m, 4H), 3.86 (m, 4H), 3.96 (s, 3H), 4.34 (t, *J* = 4.2 Hz, 2H), 5.15 (s, 2H), 7.19 (s, 1H), 7.33 (d, 1H), 7.78 (m, 2H), 8.10 (s, 1H), 8.49 (s, 1H), 8.50 (t, *J* = 4.2 Hz, 1H), 8.83 (s, 1H), 9.44 (s, 1H); ^{13}C-NMR (151 MHz, DMSO-d_6): δ (ppm): 21.63, 38.92, 52.59, 56.26, 68.09, 68.17, 68.42, 68.48, 68.97, 102.04, 108.94, 121.16, 123.36, 124.81, 130.56, 131.50, 138.78, 146.82, 148.87, 152.66, 153.43, 159.92, 161.52, 164.68.

N-(2-{2-[2-({4-[(3,4-Difluorophenyl)amino]-6-methoxy-quinazolin-7-yl}oxy)ethoxy]ethoxy}ethyl)-2-(3-nitro-[1,2,4]triazol-1-yl)acetamide (11d). Yellow solid powder with the yield of 42.2%; ESI-MS m/z = 545.20 $[M+H]^+$; GC-HRMS calcd for $C_{25}H_{26}F_2N_8O_7$ *m/z* = 589.1971 $[M+H]^+$, found: 589.1968; ^{1}H-NMR (400 MHz, DMSO-d_6): δ (ppm): 3.35 (t, *J* = 5.6 Hz, 2H), 3.57 (m, 4H), 3.86 (m, 2H), 3.98 (s, 3H), 4.28 (m, 4H), 5.15 (s, 2H), 7.22 (s, 1H), 7.42 (dd, J_1 = 18.8 Hz, J_2 = 7.6 Hz, 1H), 7.56 (m, 1H), 7.84 (s, 1H), 8.09 (m, 1H), 8.50 (s, 1H), 8.54 (t, *J* = 5.6 Hz, 1H), 9.61 (s, 1H); ^{13}C-NMR (101 MHz, DMSO-d_6): δ (ppm): 39.51, 53.09, 56.66, 68.43, 68.48, 68.89, 68.95, 69.42, 102.30, 108.31, 109.28, 111.36 (d, $^2J_{C\text{-}F}$ = 22.4 Hz), 117.28 (d, $^2J_{C\text{-}F}$ = 16.6 Hz), 118.48, 137.03 (d, $^3J_{C\text{-}F}$ = 8.6 Hz), 145.47 (dd, $^1J_{C\text{-}F}$ = 237.4 Hz, $^2J_{C\text{-}F}$ = 11.1 Hz), 147.44, 148.10, 148.98 (dd, $^1J_{C\text{-}F}$ = 241.4 Hz, $^2J_{C\text{-}F}$ = 11.1 Hz), 149.38, 153.16, 153.92, 156.39, 162.40, 165.41; ^{19}F-NMR (376 MHz, DMSO-d_6) : δ (ppm): -137.71 (d, $^3J_{F\text{-}F}$ = 23.2 Hz), -145.07 (d, $^3J_{F\text{-}F}$ = 23.2 Hz).

4.2 Molecular docking section

Docking studies of compound **10a** with EGFR (PDB ID: 4I23) and VEGFR-2 (PDB ID: 2RL5) were performed using vandetanib as a comparison. The molecular docking procedure was performed by the Glide Dock method using Schrödinger software (Schrödinger Corp., New York, NY, USA) as previously described [12]. Docking results were visualized using Chimera software (version number: 1.13).

4.3 Biological test section

All cell lines mentioned above were purchased from Cell Bank of China Science Academy (Beijing, China). The above cells were cultured in RPMI-1640 (Gibco Corp., USA) with 10% fetal calf serum. VEGFR-2 (Carna, Cat.No 08-191,), EGFR (Carna, Cat.No 08-115), Peptide FAM-P22 (GL Biochem, Cat. No. 112393), ATP (Sigma, Cat. No. A7699-1G) and staurosporine (MCE, Cat. No. HY-15141) were used for kinase inhibitory assay. CCK-8 assay kit (BestBio Corp., Shanghai, China) were applied in in vitro anti-proliferative assays. Primer sequences of

VEGF and β-actin (Sangon Corp., Shanghai, China) were used for VEGF/EGF gene expression inhibition tests. Cobalt chloride hexahydrate was purchased from Sigma-Aldrich (St. Louis, MO, USA). All of the test compounds were dissolved in DMSO for use.

4.3.1 Kinase inhibitory assay

14 target compounds, LYL-10 and vandetanib were screened in vitro using staurosporine as the reference compound. Tested compounds and reference compound were dissolved in DMSO to obtain drug solutions with different concentrations of 40 μM, 10 μM, 2.5 μM, 625 nM, 156 nM, 39 nM, 10 nM, 2 nM, 1 nM and 0.2 nM. Transfer 10 μL of the compound from the source plate to a new 96-well plate as the intermediate plate. Add 90 μL of 1x kinase buffer (50 mM HEPES, pH 7.5, 0.0015% Brij-35) to each well of the intermediate plate. Mix the compounds in an intermediate plate for 10 min on a shaker. Transfer 5 μL of each well from the 96-well intermediate plate to a 384-well plate in duplicates. 10 μL of 2.5 x enzyme solutions were added to each well of the 384-well assay plate and incubated at room temperature for 10 min; then 10 μL of 2.5 x peptide solution were added to each well of the 384-well assay plate and incubated at 28 °C for a specified period. 25 μL of stop buffer (100 mM HEPES, pH 7.5, 0.015% Brij-35, 0.2% Coating Reagent, 50 mM EDTA) were added to stop reaction. Collect conversion data from Caliper program; convert conversion values to inhibition values by Equation (1):

$$\text{Percent inhibition (\%)} = (\text{max-conversion})/(\text{max-min}) \times 100. \quad (1)$$

where "max" stands for DMSO control; "min" stands for low control.

Fit the data in XLFit excel add-in version 5.4.0.8 to obtain IC_{50} values by Equation (2):

$$Y=\text{Bottom} + (\text{Top-Bottom})/(1+(IC_{50}/X)^{\wedge}\text{HillSlope}) \quad (2)$$

4.3.2 *In vitro* anti-proliferative assay in hypoxia and normoxia

Evaluation of the anti-proliferative activity in hypoxia and normoxia of the compounds was performed using the CCK-8 assay as previously described [12]. In hypoxic + irradiation group, cobalt (II) chloride solution was added (except for blank group and $\text{control}_{\text{no } CoCl_2}$ group) and incubated for 24 h, then was irradiated at the dose of 8 Gy for another 24 h at 37 °C in 5% CO_2, 20 μL CCK-8 solution was added to per well and incubated for another 1 h. Measured absorbance at 450 nm in a plate reader and calculated for inhibition ratios.

Hypoxic sensitive enhancement ratios ($HSER_{\text{hyp}}$) were calculated using Equation (3):

$$HSER_{\text{hyp}} = \frac{Ir_{hyp}}{Ir_{nor} + (1 - Ir_{nor}) \times Ir_{CoCl_2}} \quad (3)$$

Where Ir_{hyp} and Ir_{nor} mean the inhibition ratios of target compounds or vandetanib in hypoxia and normoxia; $\text{Ir}_{\text{CoCl}_2}$ means the inhibition ratios of $CoCl_2$ group and $CoCl_2$+irradiation group on A549 and H446 cells.

Irradiation-hypoxic sensitive enhancement ratios ($HSER_{\text{hyp+IR}}$,) was calculated using Equation (4):

$$HSER_{\text{hyp+IR}} = \frac{Ir_{hyp+IR}}{Ir_{\text{hyp}} + \left(1 - Ir_{\text{hyp}}\right) \times Ir_{CoCl_2+\text{IR}}} \quad (4)$$

Where Ir_{hyp+IR} means the inhibition ratios of target compounds or vandetanib in hypoxia+irradiation; $\text{Ir}_{\text{CoCl}_2+\text{IR}}$ means the inhibition ratios of $CoCl_2$+irradiation group on A549 and H446 cells.

4.3.3 *In vitro* VEGF gene expression inhibition assays

Evaluation of the VEGF gene expression levels in hypoxia and normoxia of the compounds was performed as previously described[12].

4.3.4 *In vivo* anticancer activity assay

Mice were orthotopically implanted with *in vitro* cultured A549 cells (1×10^7 cells per mouse). After 6 or 7 days of cell inoculation, mice were divided into groups, and the administration of tested compounds was started.

Tumor dimensions were measured using a caliper, and the body weight of animals was monitored daily. Tumor volume (mm^3) was calculated using the formula ($a^2 \times b$)/2, where a = shortest tumor diameter in millimeters, and b = longest tumor diameter in millimeters. Tumor growth inhibition (TGI) was calculated using Equation (5):

$$TGI\ (\%) = [1-(V_t-V_0)/(V_{ctrl}-V_{ctrl-0})] \times 100$$

Where V_t means tumor volume of treated mice and V_{ctrl} that untreated control animals; V_0 and V_{ctrl-0} mean tumor volumes of treated mice and control animals at the day starting the administration.

Ethics statement

The study was approved by the Institutional Animal Ethical Committee of the Institute of Radiation Medicine (Peking Union Medical College & Chinese Academy of Medical Sciences, China). Animal welfare and experimental procedures were followed in accordance with the Guide for Care and Use of Laboratory Animals (National Institutes of Health, US).

Acknowledgments

This work was supported by the National Natural Science Foundation of China (31670859), CAMS Innovation Fund for Medical Sciences (CIFMS 2016-I2M-3-022 and 2017-I2M-3-019) and Fundamental Research Funds for the Central Universities (3332018117).

Conflict of interest

The authors declare no conflict of interest.

References:

[1]. (a) D. S. Krause, R. A. Van Etten, Tyrosine kinases as targets for cancer therapy. *N. Engl. J. Med.* 353 (2005) 172-187. (b) K. S. Bhullar, N. O. Lagarón, E. M. McGowan, I. Parmar, A. Jha, B. P. Hubbard, H. P. V. Rupasinghe, Kinase-targeted cancer therapies: progress, challenges and future directions. *Mol. Cancer* 17 (2018) 48-68.

[2]. (a) C. Widakowich, G. de Castro, Jr., E. de Azambuja, P. Dinh, A. Awada, Review: side effects of approved molecular targeted therapies in solid cancers. *Oncologist* 12 (2007) 1443-1455; (b) F. A. L. M. Eskens, J. Verweij, The clinical toxicity profile of vascular endothelial growth factor (VEGF) and vascular endothelial growth factor receptor (VEGFR) targeting angiogenesis inhibitors; A review. *Eur. J. Cancer*. 42 (2006) 3127-3139; (c) H. Izzedine, S. Ederhy, F. Goldwasser, J. C. Soria, G. Milano, A. Cohen, D. Khayat, J. P. Spano, Management of hypertension in angiogenesis inhibitor-treated patients. *Ann. Oncol*. 20 (2009) 807-815.

[3]. (a) D. R. Shah, R. R. Shah, J. Morganroth, Tyrosine kinase inhibitors: their on-target toxicities as potential indicators of efficacy. *Drug Safety.* 36 (2013) 413-426; (b) T. Force, D. S. Krause, R. A. Van Etten, Molecular mechanisms of cardiotoxicity of tyrosine kinase inhibition. *Nat. Rev. Cancer*. 7 (2007) 322-344.

[4]. L. Goethals, A. Debucquoy, C. Perneel, K. Geboes, N. Ectors, H. De Schutter, F. Penninckx, W. H. McBride, A. C. Begg, K. M. Haustermans, Hypoxia in human colorectal adenocarcinoma: comparison between extrinsic and potential intrinsic hypoxia markers. *Int. J. Radiat. Oncol. Biol. Phys.* 65 (2006) 246-254.

[5]. (a) C. W. Pugh, P. J. Ratcliffe, Regulation of angiogenesis by hypoxia: role of the HIF system. *Nat. Med.* 9 (2003) 677-684; (b) P. H. Maxwell, G. U. Dach, J. M. Gleadle, L. G. Nicholls, A. L. Harris, I. J. Stratford, O. Hankinson, C. W. Pugh, P. J. Ratcliffe. Hypoxia-inducible factor-1 modulates gene expression in solid tumors and influences both angiogenesis and tumor growth. *Proc. Natl. Acad. Sci. USA.* 94 (1997) 8104-8109; (c) D. Shweiki, A. Itin, D. Soffer, E. Keshet, Vascular endothelial growth factor induced by hypoxia may mediate hypoxia-initiated angiogenesis. *Nature.* 359 (1992) 843-845; (d) B. J. Moeller, Y. Cao, Z. Vujaskovic, C. Y. Li, Z. A. Haroon, M. W. Dewhirst, The relationship between hypoxia and angiogenesis. *Semin. Radiat. Oncol.*

14 (2004) 215-221.

[6]. (a) L. M. Van Putten, R. F. Kallman, Oxygenation status of a transplantable tumor during fractionated radiation therapy. *J. Natl. Cancer. I.* 40 (1968) 441-451; (b) R. F. Kallman, The phenomenon of reoxygenation and its implications for fractionated radiotherapy. *Radiology* 105 (1972) 135-142.

[7]. (a) K. De Bock, M. Mazzone, P. Carmeliet, Antiangiogenic therapy, hypoxia, and metastasis: risky liaisons, or not? *Nat. Rev. Clin. Oncol.* 8 (2011) 393-404; (b) G. Bergers, D. Hanahan, Modes of resistance to anti-angiogenic therapy. *Nat. Rev. Cancer*. 8 (2008) 592-603.

[8]. (a) I. Ott, R. Gust, Non platinum metal complexes as anti-cancer drugs. *Arch. Pharm.* 340 (2007) 117-126; (b) U. Jungwirth, C. R. Kowol, B. K. Keppler, C. G. Hartinger, W. Berger, P. Heffeter, Anticancer activity of metal complexes: involvement of redox processes. *Antioxid. Redox. Sign.* 15 (2011) 1085-1127.

[9]. C. Karnthaler-Benbakka, D. Groza, K. Kryeziu, V. Pichler, A. Roller, W. Berger, P. Heffeter, C. R. Kowol, Tumor-targeting of EGFR inhibitors by hypoxia-mediated activation. *Angew. Chem. Int. Ed. Engl.* 53 (2014) 12930-12935.

[10]. (a) J. X. Duan, H. Jiao, J. Kaizerman, T. Stanton, J. W. Evans, L. Lan, G. Lorente, M. Banica, D. Jung, J. Wang, H. Ma, X. Li, Z. Yang, R. M. Hoffman, W. S. Ammons, C. P. Hart, M. Matteucci, Potent and highly selective hypoxia-activated achiral phosphoramidate mustards as anticancer drugs. *J. Med. Chem.* 51 (2008) 2412-2420; (b) C. Karnthaler-Benbakka, D. Groza, B. Koblmüller, A. Terenzi, K. Holste, M. Haider, D. Baier, W. Berger, P. Heffeter, C.R. Kowol, B.K. Keppler, Targeting a targeted drug: an approach toward hypoxia-activatable tyrosine kinase inhibitor prodrugs. *ChemMedChem.* 11(2016) 2410-2421.

[11]. D. Das, J. Hong, Recent advancements of 4-aminoquinazoline derivatives as kinase inhibitors and their applications in medicinal chemistry. *Eur. J. Med. Chem.* 170 (2019) 55-72.

[12]. H. Q. Wei, D. G. Li, X. B. Yang, H. H. Shang, S. J. Fan, Y. L. Li, D. Song, Design and synthesis of vandetanib derivatives containing nitroimidazole groups as tyrosine kinase inhibitors in normoxia and hypoxia. *Molecules.* 21 (2016) 1693-1708.

[13]. (a) B. Melgaard, H. S. Hansen, Z. Kamieniecka, O. B. Paulson, A. G. Pedersen, X. F. Tang, W. Trojaborg, Misonidazole neuropathy: a clinical, electrophysiological and histological study. *Ann. Neurol.* 12 (1982) 10-17; (b) M. A. Stevenson, S. K. Calderwood, C. N. Coleman, Effects of nitroimidazoles on neuronal cells in vitro. *Int. J. Radiat. Oncol. Biol. Phys.* 16 (1989) 1225-1230.

[14]. (a) T. Inomata, Y. Ogawa, A. Nishioka, N. Hamada, S. Ito, S. Kariya, S. Yoshida, H. Nagasawa, H. Hori, S. Inayama, The immunopotentiation effects of the bifunctional radiosensitizer KIN-806 in comparison with its analogs KIN-804 and KIN-844. *Oncol. Rep.* 6 (1999) 1209-1221; (b) T. Inomata, Y. Ogawa, S. Ito, S. Kariya, N. Hamada, A. Nishioka, S. Yoshida, H. Nagasawa, H. Hori, S. Inayama, Lung metastasis suppression of the bifunctional new radiosensitizer KIN-806. *Int. J. Mol. Med.* 4 (1999) 257; (c) S. Kasai, H. Nagasawa, M. Yamashita, M. Masui, H. Kuwasaka, T. Oshidani, Y. Uto, T. Inomata, S. Oka, S. Inayama, H. Hori, New antimetastatic hypoxic cell radiosensitizers: design, synthesis, and biological activities of 2-nitroimidazole-acetamide, TX-1877, and its analogues. *Bioorg. Med. Chem.* 9 (2001) 453-464.

[15]. (a) K. Pasupathy, C. K. K. Nair, T. V. Kagiya, Effect of a hypoxic radiosensitizer, AK 2123 (Sanazole), on yeast *Saccharomyces cerevisiae*. *J. Radiat. Res.* 42 (2001) 217-227; (b) R. Rajagopalan, T. V. Kagiya, C. K. K. Nair, Radiosensitizer Sanazole (AK-2123) enhances γ-radiation-induced apoptosis in murine fibrosarcoma. *J. Radiat. Res.* 44 (2003) 359-365; (c) C. Sugie, Y. Shibamoto, M. Ito, H. Ogino, H. Suzuki, Y. Uto, H. Nagasawa, H. Hori, Reevaluation of the radiosensitizing effects of Sanazole and Nimorazole *in vitro* and *in vivo*. *J. Radiat. Res.* 46 (2005) 453-459; (d) S. Kapoor, R. Mathew, N. G. Huilgol, T. V. Kagiya, C. K. K. Nair, Redox reactions of Sanazole (AK-2123) in aqueous solutions: a pulse radiolysis study. *J. Radiat. Res.* 41 (2000) 355-366. (e) W. Dobrowskya, N. G. Huigolb, R. S. Jayatilakec, N. Kizilbashd, Sait Okkane, V. T.

Kagiyaf, H. Tatsuzaki, AK-2123 (Sanazol) as a radiation sensitizer in the treatment of stage III cervical cancer: Results of an IAEA multicentre randomised trial. *Radiother. Oncol.* 82 (2007) 24-29.

[16]. (a) R. S. Herbst, M. S. Kies. ZD1839 (Iressa) in non-small cell lung cancer, *Oncologist*, 2002, 7 (Suppl 4): 9215; (b) V. Grunwald, M. Hidalgo. Development of the epidermal growth factor receptor inhibitor Tarceva (OSI2774), *Adv. Exp. Med. Biol.*, 2003, 532: 235-246.

[17]. L. F. Hennequin, E. S. E. Stokes, A. P. Thomas, C. Johnstone, P. A. Ple, D. J. Ogilvie, M. Dukes, S. R. Wedge, J. Kendrew, J. O. Curwen, Novel 4-anilinoquinazolines with C-7 basic side chains: design and structure activity relationship of a series of potent, orally active, VEGF receptor tyrosine kinase inhibitors. *J. Med. Chem.* 45 (2002) 1300-1312.

[18]. J. C. Hancox, A. F. James, Refining insights into high-affinity drug binding to the human ether-à-go-go-related gene potassium channel. *Mol. Pharmacol*, 73 (2008) 1592-1595.

Highlights

- Fourteen novel 4-anilinoquinazoline derivatives containing 3-nitro-1,2,4-triazole moiety with dual EGFR/VEGFR-2 kinase inhibitory activities were designed and synthesized.

- Lead compounds, **10a** and **10g,** showed enhanced anti-proliferative activity on cancer cells under hypoxia compared to vandetanib.

- **10a** and **10g** not only inhibited tumor growth in A549 xenografts but also significantly reduce toxicity associated with weight loss compared to vandetanib.